



# Zero-Waste Approach: Assessment of Aluminum-Based Waste as a Photocatalyst for Industrial Wastewater Treatment Ecology

Rahma Hussien Thabet<sup>1</sup> · Mai Kamal Fouad<sup>2</sup> · Shakinaz Aly El Sherbiny<sup>2</sup> · Maha Abdelbaset Tony<sup>1</sup>

Received: 4 November 2021 / Revised: 16 March 2022 / Accepted: 5 May 2022 / Published online: 31 May 2022  
© The Author(s) 2022

## Abstract

Alum sludge (AS) is produced in inevitable amounts from drinking water treatment plants. Also, dye-contaminating wastewater is usually discharged from textile industries that must be treated to meet the environmental authorities; thus, Fenton's reagent is a suitable candidate. However, reducing the quantity of chemicals used in Fenton reactions can be partly achieved by an industrial ecology approach. This paper is introducing alum sludge waste as a photocatalyst, (termed as AS-Fenton), that is prepared under mild experimental conditions. Thermogravimetric and differential thermogravimetric analyses were conducted to attain full illustrations of the thermal treatment steps. Its chemical composition and morphology is revealed using X-Ray Diffraction and Scanning Electron Microscope. Thus, this research is of great significance for the application of a waste by-product for being a Fenton source for photocatalytic removal of Levafix Blue dye effluent. A new modified Fenton reagent was applied with the addition of 1.0 g/L and 800 mg/L of catalyst and H<sub>2</sub>O<sub>2</sub>, respectively, at pH 3.0 shows high potential for the dye removal. The starting concentration of the Levafix Blue CA was halved during the first 5 min under the UV illumination. The most effective operating variables are optimized through Response Surface Methodology. The kinetics of the dye removal was investigated and the reaction following the pseudo-first-order regime with the kinetic constant ( $K_p$ ), ranged in 0.04–0.57 min<sup>-1</sup>. Thermodynamic parameters reveal that the reaction is a non-spontaneous and endothermic in nature. Hence, toxicity of the dye is significantly reduced via Fenton reaction to non-toxic end products.

## Article Highlights

- Water treatment sludge comprises zeolite, quartz and calcium aluminum silicate
- Calcined alum sludge could be used as a source of photo catalyst
- Fenton oxidation is proposed for treating Levafix CA dye and showed almost complete dye oxidation
- RSM was applied to optimize Fenton process parameters

**Keywords** Levafix Blue dye · Oxidation · Reaction kinetics · Alum sludge · Thermodynamics · Optimization

## Introduction

Globally, there is an urgent worldwide demand for clean drinking water (Tony 2021b). Therefore, coagulation and flocculation techniques are essential in water industry sector as pre-treatment steps (Zhao et al. 2009). Conventionally, aluminum salts have been applied to attain such purposes for several decades (Lv et al. 2015). The result is generating a huge volume of aluminum-based sludge around the world, namely, alum sludge. Aluminum-based sludge by-product is generally produced in drinking water treatment plant as 3% (by volume) of the raw water (Kasina et al. 2019). Moreover,

✉ Maha Abdelbaset Tony  
dr.maha.tony@gmail.com

<sup>1</sup> Advanced Materials/Solar Energy and Environmental Sustainability (AMSEES) Laboratory, Basic Engineering Science Department, Faculty of Engineering, Menoufia University, Shebin El-Kom, Egypt

<sup>2</sup> Chemical Engineering Department, Faculty of Engineering, Cairo University, Giza, Egypt

the thickened sludge containing a solid content ranged from 2 to 4% that may be increased in the mechanically thickened sludge to reach to an estimated value of 23% solid content (Tantawy 2015; Tony et al. 2011). On the other hand, there is a lack in the information regarding the global or national aluminum-based sludge production and disposal. For instance, in Egypt, the statistics data associated with aluminum-based sludge levels and costs are limited. In the meantime, a key perennial issue related to the aluminum-based sludge is its efficient disposal in a sustainable and economic potential (Tony and Lin 2021). Due to the massive sludge amounts and its environmental drawbacks that ultimately affect urban pollution and watercourse, searching for an engineering solution is a research topic.

Hence, several researchers and industries have questioned the feasibility of attaining a viable sustainable management option for alum sludge. However, with the global attention for a sustainable and eco-friendly environment, managing alum sludge is gaining a special concern (Zhao et al. 2021). Imperative financial and environmental costs are forcing the industrial sector to develop alternative management strategies and the answer must be “recycling, reuse and resource recovery” (Parker et al. 2012; Tony 2019b). Aluminum-based sludge utilization can be considered as an alternative option to manage alum sludge for safe waste management. Extensive research studies have been reported in literature are dealing with investigating the possibility of using aluminum-based sludge as one of the major adsorbent materials for pollutants eliminations. For instance, alum sludge could be applied to eliminate a wide range of dyes (Chu 2001), phosphorus (Liu et al. 2016) and recently, it is successfully applied to remove some inorganic heavy metals from wastewater such as chromium (Liu et al. 2013).

Not only alum sludge discharged into the environment, but also dyes are released into the environment as part of many industrial discharges, including leather industry, textile manufacturing, paper industries, and paints industries (Ashour and Tony 2017). Textile industry is considered as one of the most polluting sectors in terms of effluent type and amount that pose severe environment hazards (Bansal and Verma 2017; Tony and Mansour 2019; Tony et al. 2019). The discharge of such toxic and carcinogenic effluents to the water bodies cause a severe damage to the aquatic ecosystems and consequently cause damage to humans and other living creatures (Ashour and Tony 2020). Even very low dye concentrations in the wastewater that may be less than 1 ppm are potentially posing significant threat to the biosphere; so, for a safe disposal, they should be removed from wastewater effluents before the final discharge. Scattered studies have been reported that the feasibility of aluminum-based sludge materials to remove dyes from the textile discharge effluents (Dassanayake et al. 2015). However, according to the data available there is a few literature cited including the recent

literature regarding the utilization of alum sludge as a photocatalyst material.

Advanced oxidation processes (AOPs) based on photocatalysis are reliable and abundantly applied catalysts for toxicity remediation since they are capable of oxidizing a wide variety of pollutants in wastewater effluents due to a range of chemical interactions (Papoulis 2019). It has been reported that Fenton reaction is extensively applied as a photocatalytic reaction that utilizing iron oxides and hydrogen peroxide to generate highly oxidant intermediates, namely OH radical (Tony 2021c). Much research have been conducted based on iron and copper Fenton reaction, however, also other transition metal ions, i.e., Zn(II), Co(II), Cr(III), Ni(II) and Mn(II) role is of interest (Ghorpade and Ahammed 2018; Strlic et al. 2003; Tony et al. 2009). Moreover, aluminum sludge is also applied as a Fenton reaction according to the previous reported studies. In the last decades, previous study (Ruipérez et al. 2012) demonstrated the application of aluminum-based Fenton reaction to overcome the drawbacks of Fenton reaction. Moreover, Exley (2004) used a non-iron-mediated oxidation based on aluminum Fenton system to produce hydroxyl radicals oxidants for pollutants remediation. Nguyen et al. (2021) promoted electro-Fenton reaction using alum sludge from drinking water treatment plant residuals. Aluminum, Al, is recognized as one of the most abundant metals in the earth's crust that is able to form diverse strong complexes (Geng et al. 2018). Aluminum displays a promising pro-oxidation activity. Previous reports suggested that the formation of the Al-superoxide,  $O_2^{\cdot-}$  radical, is related to the metal oxidant activity (Ruipérez et al. 2012).

Economic aluminum-based sludge disposal and its sustainable reuse is an environmental concern. Thus, utilizing such by-product to be a photocatalyst to treat another industrial waste is an industrial ecology approach. In our recent publication (Tony 2020b), results have already shown that alum sludge is an efficient adsorber for industrial wastewater remediation such as dyes; however, its affinity to be a photocatalyst has not been investigated for Levafix dye removal from aqueous stream. Thus, alum sludge that is comprising of both aluminum and iron could be introduced as a Fenton source.

To the best of the authors' knowledge, although there is a limited reported data in the literature investigating the preparation of calcined aluminum-based sludge from drinking water treatment plant for further applications, there is a lack in exploring the calcined alum sludge as a photocatalyst in its simple preparation form.

Herein, the feasibility of different alum sludge-based catalysts namely, AS, AS400, AS600 and AS800 for dye removal from aqueous solutions have been investigated and presented. The various characterizations of such materials are displayed. To add up, the effect of different oxidation

technology is investigated. Various kinetic modeling were applied and thermodynamic parameters were estimated to determine the mechanism of alum/Fenton system oxidation of such materials. Initial results of various operating parameters are promising as a potential technology for not only recommending the reuse of the alum sludge waste, but also for the efficient treatment of the dye-contaminating wastewater. Furthermore, optimizing the removal efficiency in terms of most effective factors, namely alum sludge dose, hydrogen peroxide concentration and pH, where the dye removal is considered the target response to derive the quadratic model based on Box–Behnken design (BBD) of the response considering the joint effects of the operating factors, and for further depict the response surface for each case to locate the optimal conditions based on the overlay plot.

## Materials and Methods

### Materials

All materials were used as received without further purification. Levafix Blue CA dye was supplied by DyStar Ltd., German is used as source of simulated wastewater contaminated with reactive textile dye effluent. Levafix CA is bifunctional and combined anchor (CA) that reveals the existence of chlorine-free tri-fluoropyrimidine, mono-fluorotriazine and new vinyl sulfone anchor groups (Brock 2004). Sulfuric acid and sodium hydroxide of analytical grades were supplied for the pH adjustment to the required value. 30% w/w hydrogen peroxide ( $H_2O_2$ ) was used as the source of initiating the AS-Fenton's reaction.

### Preparation of Alum Sludge-Based Fenton Catalyst

Alum sludge as a by-product residue from the drinking water treatment plant was collected from Gezirat El Dabh treatment plant, Giza governorate, Egypt. The raw water pumped through the plant from the River Nile reservoir. The plant uses aluminum sulfate as a primary coagulant for flocculating reservoir water and therefore, aluminum-based sludge is produced as a by-product. Alum sludge used in the present study was directly collected from the underflow channel of the sedimentation tank to further treatment for reuse according to the procedure that is previously stated elsewhere (Tony 2020b). Afterwards, the collected alum sludge is transported into the laboratory and subjected to gravity settling in order to eliminate the excess water. Then, the sludge is subjected to air-drying to diminish the moisture content to about 10%. The obtained sludge cake is then washed to eliminate any impurities before it is exposed to overnight oven drying ( $105\text{ }^\circ\text{C}$ ) to remove any water content before storing for further use. The washed and dried alum

sludge is exposed for grinding via ball mill grinding (1 h), and the sample is referred as (AS). Afterwards, AS is then calcined in an electrical furnace at a rate of  $10\text{ }^\circ\text{C}/\text{min}$  for 2 h at different temperatures ( $400$ ,  $600$  or  $800\text{ }^\circ\text{C}$ ), and the resultant samples after calcination are labeled as AS400, AS600 or AS800, respectively. Graphical overview of the AS calcination and the corresponding surface functionality is illustrated in Fig. 1.

### Photocatalytic Test

The model solution of 100 ppm of Levafix Blue CA and the certain amount of the alum sludge type and hydrogen peroxide as the sources of the photocatalyst was placed in the reactor, magnetically stirred and kept under the UV at the wavelength of 231 nm until the steady state or complete dye removal is achieved. The samples were collected, in regular time intervals, for every 10 min. Filtered samples by syringe filters (0.45 mm) were analyzed using UV–visible spectrophotometer, Model Unico UV-2100, USA. For comparison, solo  $H_2O_2$  and alum sludge systems were investigated and the effect of the dye load was also examined under the same conditions. The results, describing the removal of Levafix Blue CA, were presented as C/Co, where C is the Levafix Blue CA concentration determined at time t and Co is the initial Levafix Blue CA concentration. The pH of dyed wastewater samples was adjusted, if needed; using a digital pH-meter, model AD1030, Adwa instrument, Hungary. Figure 2 simply summarizes the experimental set-up.

### Characterization Study

The morphologies of the prepared AS samples were explored and imaged by field-emission scanning electron microscope (SEM) (FE-SEM, Quanta FEG 250). The used

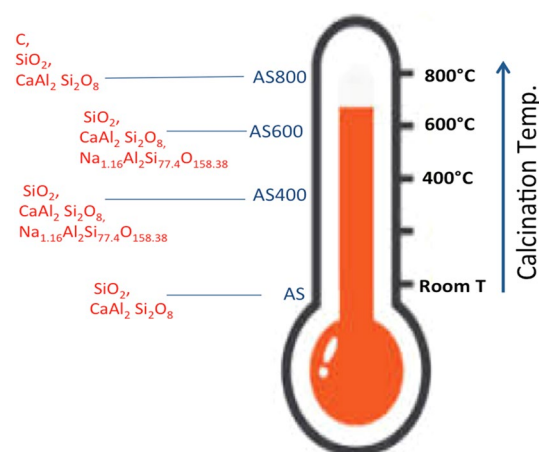


**Fig. 1** Development of the surface functionality of AS upon calcination

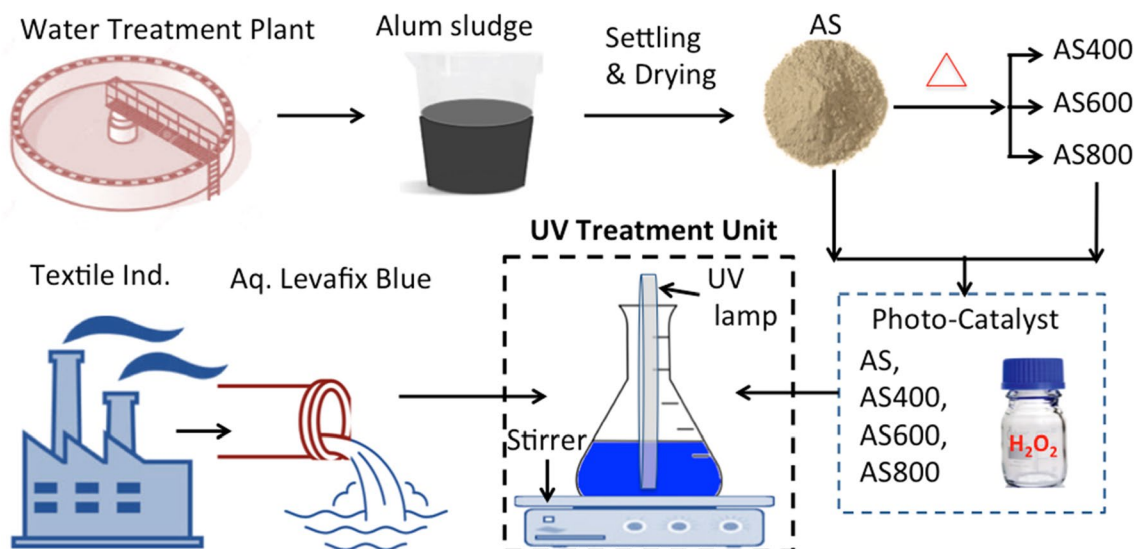


Fig. 2 Schematic representation of the experimental set-up

typical magnifications were 8000 × and 60,000 ×. This was accompanied by energy-dispersive X-ray spectroscopy (EDX). The main oxides contented in the alum sludge were assessed by energy-dispersive spectrum. The crystal structure of the prepared alum sludge photocatalyst samples, i.e., AS, AS400, AS600 and AS800 was characterized using an XRPhillips X’pert (MPD3040) diffractometer using Cu Ka radiation source ( $\lambda = 1.5406$ ) run at 40 kV and 40 mA. The obtained intensity of the diffracted X-rays is recorded at step-scan mode of 0.02°. Thermal stability of the sludge samples was analyzed using thermogravimetric analysis (TGA) to determine the mass losses of the alum sludge samples. During TGA analysis, alum sludge was heated to 800 °C at a constant rate of 10 °C/min in a nitrogen atmosphere was conducted using a DTG-60H type.

**BBD**

To attain a full understanding of the role of the most significant measured independent parameters on the Levafix CA removal as Levafix Blue color removal percentage, dependent variables, a three-level of factorial design with triplicates of the central values, namely Box–Behnken design (BBD), was investigated based on response surface methodology (RSM). The selected independent variables were chosen according to the most influenced factors according to the following: (1) pH value; (2) AS400 concentration and (3) H<sub>2</sub>O<sub>2</sub> dose. The boundaries of each BB factor are determined from the preliminary experiments as guidance and the data displayed in Table 1.

The full factorial experimental matrix was designed according to the statistical analysis software (SAS, Institute USA) and the 15-runs of experimental design with the

Table 1 BBD boundaries of the experimental domain and spacing of levels in their coded and natural units for Levafix CA removal

Variable	Symbols <sup>a</sup>		Range and levels		
	Natural	Coded	- 1	0	1
pH	$\vartheta_1$	$\delta_1$	2.5	3.0	3.5
AS400 (mg/L)	$\vartheta_2$	$\delta_2$	0.5	1.0	1.5
H <sub>2</sub> O <sub>2</sub> (mg/L)	$\vartheta_3$	$\delta_3$	600	800	1000

<sup>a</sup>Code level ( $\delta_1 = (\vartheta_1 - 3.0)/0.5$ ,  $\delta_2 = (\vartheta_2 - 1.0)/0.5$ ,  $\delta_3 = (\vartheta_3 - 800)/200$ )

results of the BBD are listed in Table 2. Additionally, statistical and graphical analyses were investigated using SAS (SAS, Institute USA) and Matlab (7.11.0.584), respectively. Also, analysis of variance, ANOVA, was listed to investigate the significance of the statistical model.

A quadratic second-order polynomial model was used to describe the model relationship between the percentage of the dye removal (the dependent variable) and the operating independent variables (i.e., pH; AS400 concentration and H<sub>2</sub>O<sub>2</sub> dose) and the corresponding quadratic polynomial equation is given as the following Eq. (1):

$$\gamma = \beta_o + \sum \beta_i \delta_i + \sum \beta_{ii} \delta_i^2 + \sum \sum \beta_{ij} \delta_i \delta_j, \tag{1}$$

where  $\gamma$  is the predicted Levafix Blue CA removal rate as the dependent response (%);  $i = 1, 2, 3$  and  $j = 1, 2, 3$ ;  $\beta_o, \beta_i, \beta_{ii}$  and  $\beta_{ij}$  are the model regression coefficient parameters; and  $\delta_i$  is the input controlling coded variable. The natural values of the operating parameters ( $\vartheta_i$ ) were assigned as coded variables ( $\delta_i$ ) in accordance with Eq. (1) (Montgomery 2017) to simplifying the model calculations. The optimum values

**Table 2** BBD for the three experimental variables and its responses

Exp. no.	Variables						Response ( $\gamma$ , %)	
	pH		AS400 concentration		H <sub>2</sub> O <sub>2</sub> dose		Experimental	Predicted
	Coded	Natural	Coded	Natural	Coded	Natural		
1	-1	2.5	-1	0.5	0	600	87.03	85.30
2	-1	2.5	1	1.5	0	1000	91.21	92.68
3	1	3.5	-1	0.5	0	600	40.42	38.94
4	1	3.5	1	1.5	0	1000	41.72	43.44
5	0	3	-1	0.5	-1	600	57.89	58.56
6	0	3	-1	0.5	1	1000	61.98	64.49
7	0	3	1	1.5	-1	600	68.66	66.14
8	0	3	1	1.5	1	1000	69.46	68.78
9	-1	2.5	0	1	-1	600	90.82	91.86
10	1	3.5	0	1	-1	600	39.62	40.42
11	-1	2.5	0	1	1	1000	93.31	92.51
12	1	3.5	0	1	1	1000	49.40	48.35
13	0	3	0	1	0	800	68.06	69.92
14	0	3	0	1	0	800	69.86	69.92
15	0	3	0	1	0	800	71.86	69.92

were located using Mathematica software (V 5.2). Further, three additional replicates were conducted according to the theoretical optimum values to validate the prediction model.

## Results and Discussions

### Characterization of the Prepared AS-Based Materials

X-ray diffraction (XRD) patterns of the prepared samples are displayed in Fig. 3 to investigate the mineral composition of the raw alum sludge (AS) sample and the thermally treated alum sludge at 400, 600 and 800 °C. It is revealed from the XRD pattern that quartz (silicon oxide, SiO<sub>2</sub>), which has a hexagonal crystal shape, is the predominant crystalline inorganic substance in such materials since the most intensive SiO<sub>2</sub> peaks are allocated according to its *hkl* planes as illustrated from the Fig. 3. Hence, water treatment facility uses solely aluminum sulfate as a primary coagulant, the suspended elements in the raw water, such as sand and clay might be the source of those quartz particles (Fungaro and Silva 2014).

Additionally, according to the observed peaks in Fig. 3, anorthic crystal structure of calcium aluminosilicate (CaAl<sub>2</sub>Si<sub>2</sub>O<sub>8</sub>) occurs in the four alum sludge samples, AS, AS400, AS600 and AS800 with a notable rise in its quantity with increasing calcination temperature. This could be illustrated by the calcination of CaCO<sub>3</sub> and Al<sub>2</sub>Si<sub>2</sub>O<sub>5</sub>(OH)<sub>4</sub>, which may aid in the formation of additional CaAl<sub>2</sub>Si<sub>2</sub>O<sub>8</sub> at AS600 and AS800 samples (Baltakys et al. 2007). To add

up, Graphite (C) crystals appear in raw AS and calcined AS samples. The crystalline-rich silica zeolite, ZSM-12 (sodium aluminum silicate, Na<sub>1.16</sub>Al<sub>2</sub>Si<sub>77</sub>40O<sub>158.38</sub>) with a monoclinic crystal structure appears in the sludge calcined at 400 °C (AS400). The primary zeolite precursors are Si and Al with Si/Al in a molar ratio of 1–1.25 (Ren et al. 2012; Rozhkovskaya et al. 2021a). Such elements are occurring in abundance in alum sludge due to the presence of sand and the usage of alum with NaOH in water treatment plants during the raw water treatment facilities. Calcination of such precursors at 400 °C results in the production of zeolite which is commonly produced around 500 °C (Espejel-Ayala et al. 2014), that could be distinguished through the presence of its *hkl* in Fig. 3 for the XRD pattern of AS400; however, it does not appear in raw sludge (AS).

On the other hand, increasing the calcination temperature over 400 °C has a negative effect on zeolite, ZSM-12, production, and its peaks vanished in the AS600 and AS800. This is most likely due to the zeolite formation that is influenced by both the Si and Al ratios. Also, the loss of ignition (Barrer 1982) also affect its presence. Moreover, the amount of quartz present in the samples is noticeably affected with the calcination temperature since its amount increases by the rise in the calcination temperature. This might be explained by the amorphous silica could crystallizes into quartz at a temperature about 245 °C (Tony 2020b). Hence, the result of sludge calcination at 400 °C, the formation ZSM-12 is formed (Rozhkovskaya et al. 2021a).

Scanning electron microscopy (SEM) was applied to describe the morphologies of both raw sludge waste sample (AS) and calcinated sludge AS400, AS600, and AS800 and

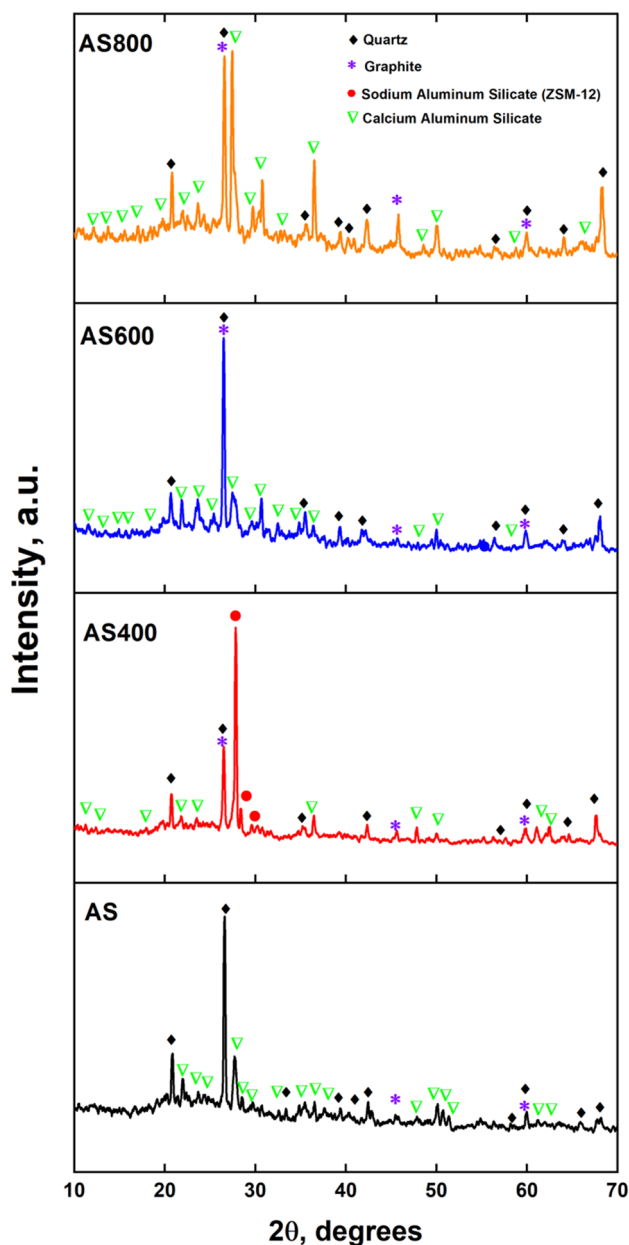


Fig. 3 X-ray diffraction of different alum sludge samples

images are given in Fig. 4. As seen in Fig. 4, the morphologies of raw (Fig. 4A) and calcinated sludge (Fig. 4B–D) surfaces were quite similar, with a porous surface structure (Nguyen et al. 2021) since the surface was dominated with a glass phase of aluminosilicate (Tony 2020a, b). Moreover, the Figure displays that the sludge shape was irregular and heterogeneous with a porous texture.

The distribution of the particle size is also evaluated using IMAGEJ 1.48 V program and illustrates that the AS400 sample attained the particle size distribution range from 0.2 to 0.8  $\mu\text{m}$  as given in Fig. 4. The typical mean particle size is 0.541  $\mu\text{m}$  with a predominant

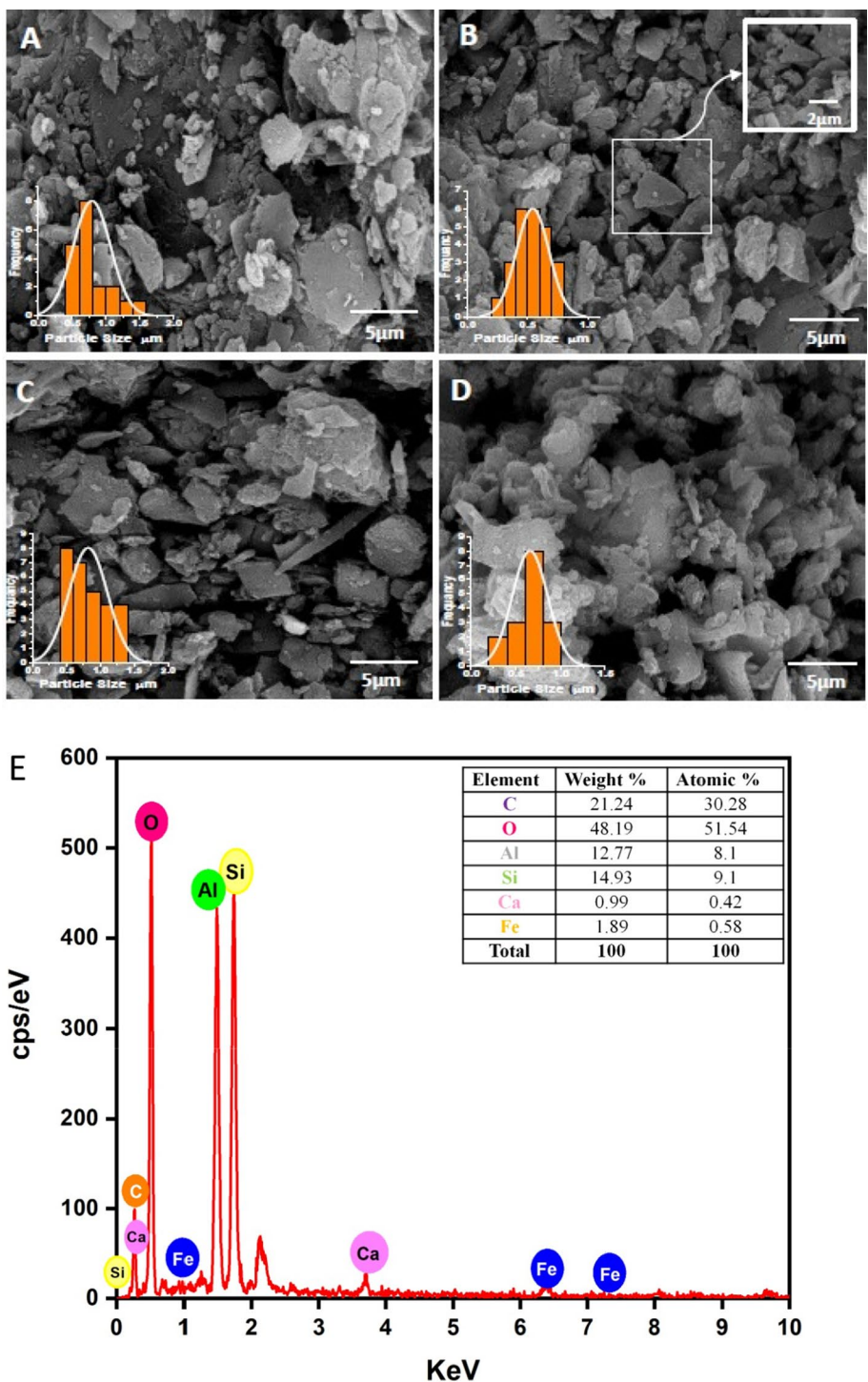
size of 0.544  $\mu\text{m}$ . Compared to other alum sludge samples that possess the following particle size range: 0.4–1.4  $\mu\text{m}$  for AS; 0.4–1.6  $\mu\text{m}$  for AS600 and 0.2–1  $\mu\text{m}$  for AS800. Thus, amongst the alum sludge samples, AS400 have a low particle size range in comparison to the other particulates of other sludge samples that allow it to have the highest surface area. Generally, high surface area helps in conducting an efficient photocatalytic oxidation reactions (Viljoen et al. 2021). Moreover, the specific surface area Brunauer–Emmett–Teller (BET),  $S_{BET}$  of the prepared sample is examined and the measured value recorded 61.58  $\text{m}^2/\text{g}$ . Such surface area is almost in accordance to the previously reported by who mentioned that the  $S_{BET}$  of water clarifier sludge is ranged from 61 to 67  $\text{m}^2/\text{g}$  (Lee et al. 2006).

EDX analysis illustrated in Fig. 4 (E) that Al, O, Si, C, Ca, and Fe are the major elements of calcined alum sludge at 400  $^{\circ}\text{C}$ , (AS400). AS400 displayed a high content of Si and Al, this could be associated to the presence of clays and aluminosilicate materials which is suitable to form Zeolite material (Rozhkovskaya et al. 2021b; Wang et al. 2019).

The thermogravimetric TGA and differential thermogravimetric analyses DTG of alum sludge were carried out and the TGA–DTA curve is given in Fig. 5. Data in Fig. 5 illustrate the results of thermal analysis of raw alum sludge (AS) sample calcination at 800  $^{\circ}\text{C}$  at 10  $^{\circ}\text{C}/\text{min}$ . The obtained thermogram results illustrate that the thermal treatment occurs in three steps: in the first step, a gradual weight loss in temperature range of 28–180  $^{\circ}\text{C}$  is corresponds to a weight loss of 8% (0.38 mg) where it is hydrated and the moisture content is lost and the reaction is endothermic reaction. In the second step, intensive (12.6%, 0.59 mg) weight loss at a temperature range of 180–414  $^{\circ}\text{C}$  and at which the decomposition of volatiles and organic matter occurs (Tantawy 2015) and the heat of reaction is recognized as exothermic reaction. At the third step, that is so-called the third step, a relative stabilization profile is occurred through endothermic reaction from 414 to 800  $^{\circ}\text{C}$  with 5.8% (0.27 mg) weight loss. At such stage, the degradation of more complex organic and carbonate matter takes place (Breesem et al. 2015) and the decomposition of inorganic compounds occurs (Shamaki et al. 2021).

Diffuse reflectant spectra (DR) is used to present a simple method for the determination of optical band gap of AS, AS400, AS600 and AS800 nanopowdered samples as shown on Fig. 6. The idea was originated from Kubelka–Munk (Eq. (2)) (Roderick 1997) which describes the behavior of light traveling inside a light scattering sample, where  $R$  is the diffuse reflectance,  $F(R)$  is called the Kubelka–Munk function, the  $E_g$  is optical band gap,  $\nu$  is light frequency,  $h$  is Plank’s constant and  $A$  is the proportionality constant.. The band gap is calculated by plotting the graph of the square product of the Kubelka–Munk function and energy ( $F(R)h\nu$ )<sup>2</sup> versus energy ( $h\nu$ ) as plotted in Fig. 7,

**Fig. 4** Joint display of SEM images of all alum sludge samples (A AS; B AS400; C AS600 and D AS800) and EDX analysis report (E) of AS400



$$(F(R)hv)^2 = A(hv - E_g). \tag{2}$$

As it appears that the direct transitions allowed are prevalent. The band gap can be obtained by extending the straight line from the straight segment of the graph touching the  $h\nu$  axis, the band gap of the sample was found to possess decreasing in values from 2.9, 1.75, 1.99 to 2.26 eV values

with corresponding to AS, AS400, AS600a and AS800, respectively. These values as they consists of Si and Al (Nassar and Abdelrahman 2017). Hence, this confirms the possibility of using such materials as photocatalysts in the visible region. Although, the current investigation is mainly conducted under the ultraviolet illumination, which possess the band gab of the ultraviolet region that is more than 2.8 eV (Yu et al. 2017), which is more than the energy required for

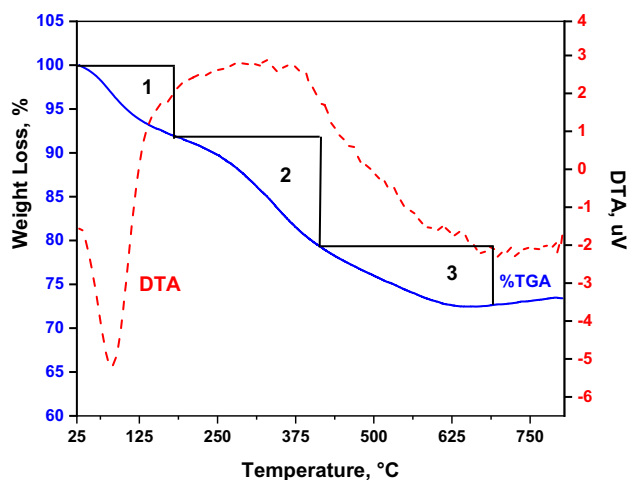


**Fig. 5** TGA/DTA thermogram of alum sludge thermally treated at 800 °C

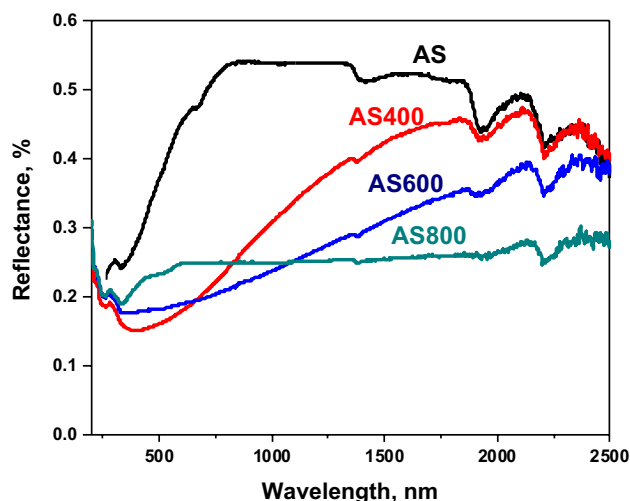


**Fig. 6** Diffuse Reflectance spectra of alum sludge powder samples

activation of such prepared materials. It is noteworthy to mention that it is predictable the activity of Fenton-based alum sludge catalyst under visible-light irradiation in real solar irradiance applications contributes to the visible-light absorption resulting in a high visible-light photocatalytic activity.

### Comparison of Different Treatment Systems on Reaction Time

Comparing of different Levafix oxidation systems are applied and the results are given in Fig. 8. The dark reaction using  $H_2O_2$ , AS400 or AS400/ $H_2O_2$  are applied for the object of comparison and the plots are compared to when using the catalyst under the ultraviolet (UV) illumination. As

seen from the graph (Fig. 8), the absence of catalyst (AS400) when using 800 mg/L  $H_2O_2$ , the extent of Levafix oxidation is barely reaches 22%. However, using AS400 only, the decrease in the Levafix Blue dye concentration is about 79% in 50 min of reaction time. This experiment reflected the contribution of the sorption/desorption equilibrium due to the presences of graphite and zeolite which have porous adsorption surfaces (Tony 2020b; Wongwichien et al. 2014). However, the addition of AS400 and  $H_2O_2$  without UV irradiation, the achieved dye oxidation is 91% removal.

To well understand the oxidation capability of AS400 as a photocatalyst, experiment using AS400 catalyst under UV illumination was conducted, whereas the photocatalytic efficiency has reached 61%. Then, adding  $H_2O_2$  to the system the efficiency was increased to maximum value 99.9% within 40-min irradiation time. This could be due to the combination of adsorption and photocatalysis processes.

Although  $H_2O_2$  is a powerful oxidant, the sample treated with solo  $H_2O_2$  could not show a significant increase in reflectance values in the visible region. In addition, the mechanism of photodegradation process (AS400 augmented UV illumination) and (AS400/ $H_2O_2$  augmented UV illumination) has been distinguished (shown in Fig. 9). The excited Levafix Blue dye molecules will convert  $O_2$  to  $O_2^{\bullet}$  when the dye molecules which absorb UV light. Then, the produced  $O_2^{\bullet}$  radicals may react with protons (generated from the autoprotolysis of water) to generate superoxide radicals,  $OOH^{\bullet}$ . Afterward, those produced radicals may eventually degrade the dye molecules completely to carbon dioxide, water and mineral acids (Nassar et al. 2014). Photocatalytic degradation of the Levafix dye molecules in the presence of AS400, under UV illumination, usually includes the separation of electron-hole pairs, which generated on the surface of zeolite present on AS400, and the subsequent reduction-oxidation reactions. The electrons can be scavenged by the adsorbed molecular oxygen species, and water or adsorbed dye molecules can trap the holes. Afterwards, LB dye molecules may be oxidized directly by the influence of photo-generated oxidants. Furthermore, adding hydrogen peroxide in the presence of AS400 and UV radiation may enhance the photodegradation rate of the dye because the direct decomposition of hydrogen peroxide under UV light generating  $OH^{\bullet}$  radicals which directly may oxidize Levafix dye molecules to carbon dioxide, water, and mineral acids (Nassar and Abdelrahman 2017).

### Comparing of Different Types of Alum Sludge/ Fenton Systems

The change in  $C/C_0$  value of Levafix dye versus irradiation time is shown in Fig. 10 for various AS samples, (AS, AS400, AS600 and AS800). It is interesting to note that the AS400 showed the highest catalytic activity compared



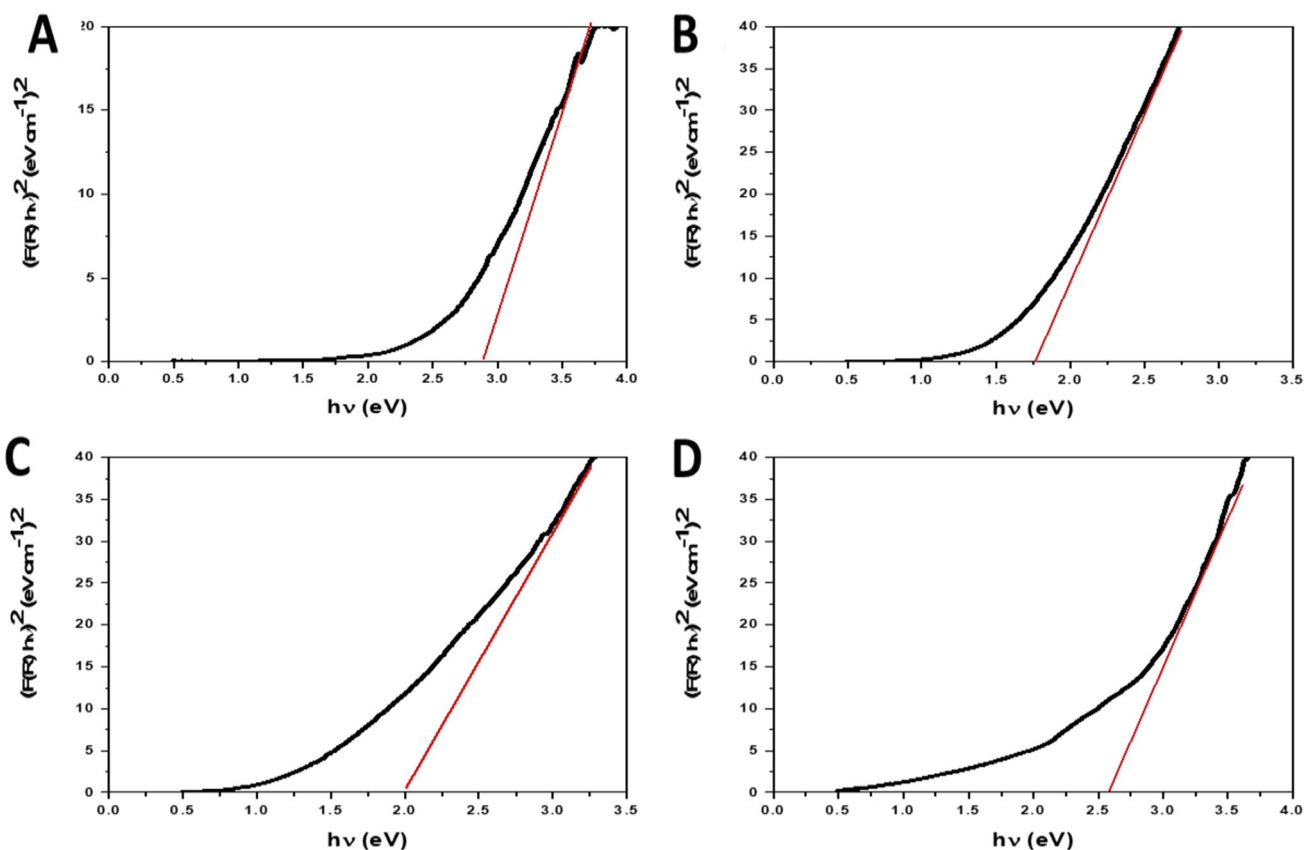


Fig. 7 Plots of  $(F(R) hv)^2$  versus  $hv$  of **A** AS; **B** AS400; **C** AS600, and **D** AS800

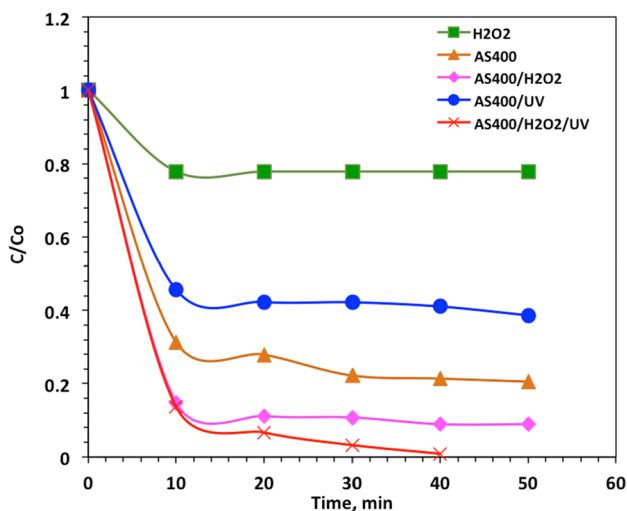


Fig. 8 Dye removal using different systems

with other samples for oxidation of Levafix dye within 30 min time of reaction. This could be attributed by the presence of sodium aluminosilicate (Zeolite) and calcium aluminosilicate in AS400, according to the X-ray diffraction result (Fig. 3), Such components are effective in dye

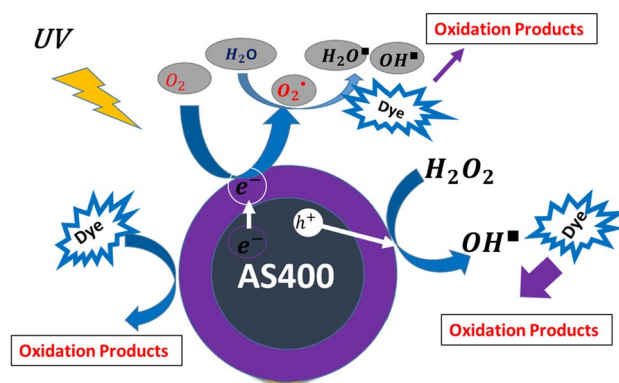
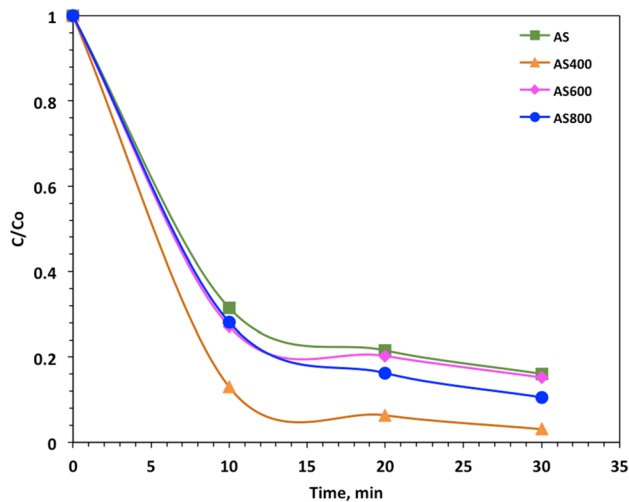


Fig. 9 Reaction mechanism for the removal of Levafix Blue dye using alum sludge (AS400) photocatalyst

adsorption and photocatalytic due to the ion exchange characteristics. Moreover, the narrow particle size distribution as supported with the SEM images (Fig. 4) helps in maximizing the oxidation efficiency that is corresponding to AS400. The above mentioned, compared to the other alum sludge samples (AS, AS600 and AS800), AS400 possess the lowest particle size range with predominant size of 0.544  $\mu\text{m}$ , which, therefore, endowed with



**Fig. 10** Effect of different alum sludge/Fenton systems on Levafix Blue dye oxidation

the highest surface area among the samples [34]. Thus, when AS400 reacted as a Fenton catalyst has a superior effect regarding its higher surface area which allow the catalyst to have more available active sites that generate more hydroxyl radicals. Such radicals are the main responsibility of the oxidation reaction. Also, the presence of aluminum on the AS400 plays an important role in modulating its photocatalytic behavior of As samples with corporation of the narrow band gap than the other 3 samples. (Wang et al. 2019).

### Effect of Initial Dye Load on AS-Fenton System

For the object of highlighting a real system applications, the effect of Levafix different initial dye concentration on the photocatalytic oxidation rate was conducted in concentration range from 60 to 200 ppm of dye solution using 800 mg/L of  $H_2O_2$ , 2 g/L of a catalyst load at pH 3.0. Figure 11 shows that as the dye solution becomes more concentrated, the photocatalytic oxidation rate tends to decrease. This indicates that there should be a maximum dye distribution allowing for a successful reaction at active sites. In addition, the dye is inefficiently adsorbed to avoid encounters with light photons, resulting in a reduction in the photodegradation rate (Thabet et al. 2020). Although the probability of photocatalyst excitation decreased at higher concentration levels, the screening effect also predominates, and hence the degradation rate decreased. However, Fig. 10 reveals that the highest percentage degradation (99.8%) of the Levafix dye occurred at the initial dye concentration of 60 ppm.

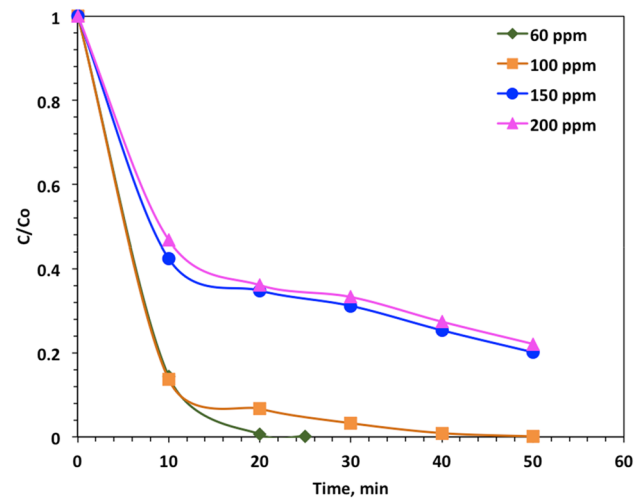


**Fig. 11** Effect of initial dye loading on the AS400/Fenton system

### Effect of Fenton Parameters

In the first set of experiments, pH of the aqueous solution besides the AS400 dose and  $H_2O_2$  concentration was studied to determine the optimal working conditions for the AS-Fenton system. The values being chosen based on Thabet et al. (2020) recommendations. First, as mentioned before, the pH of the aqueous solution plays a significant role on the dye mineralization through AS-Fenton oxidation (Tony et al. 2015). Thus, pH is one of the key considerations affecting the net charge on the surface of both the photocatalyst and the organic contaminants. Thus, the efficiency of the AS400 photocatalyst for the degradation of aqueous Levafix dye solution, with an initial dye concentration of 100 ppm, AS400 load of 2 g/L and 800 mg/L  $H_2O_2$  was studied as a function of irradiation time, at pH range of 3–10. The highest degradation efficiency of 99.9% was reached at pH 3. It can be seen from the Fig. 12A, that, as the solution media becomes more basic, the photocatalytic degradation rate of the AS400 continues to decrease due to the production of negative charge on the catalytic surface, which causes repulsion of negatively charged Levafix dye molecules (El-Desoky et al. 2010).

To obtain the optimum catalyst dose for Fenton's oxidation system, a series of four experiments were carried out at different amounts of AS400 in the range of 1–2.5 g/L with an initial Levafix dye concentration of 100 ppm, 800 mg/L  $H_2O_2$  and pH 3. The data observed in Fig. 12B shows that 1 g/L of AS400 is the optimum value corresponding to 99.9% oxidation. This could be illustrated by the presence of sufficient active sites in the reaction media. However, increasing in the catalyst load resulted in Fenton's oxidation deficiency due to the reduction of the active sites since the particles could aggregate and that hinders the surface area

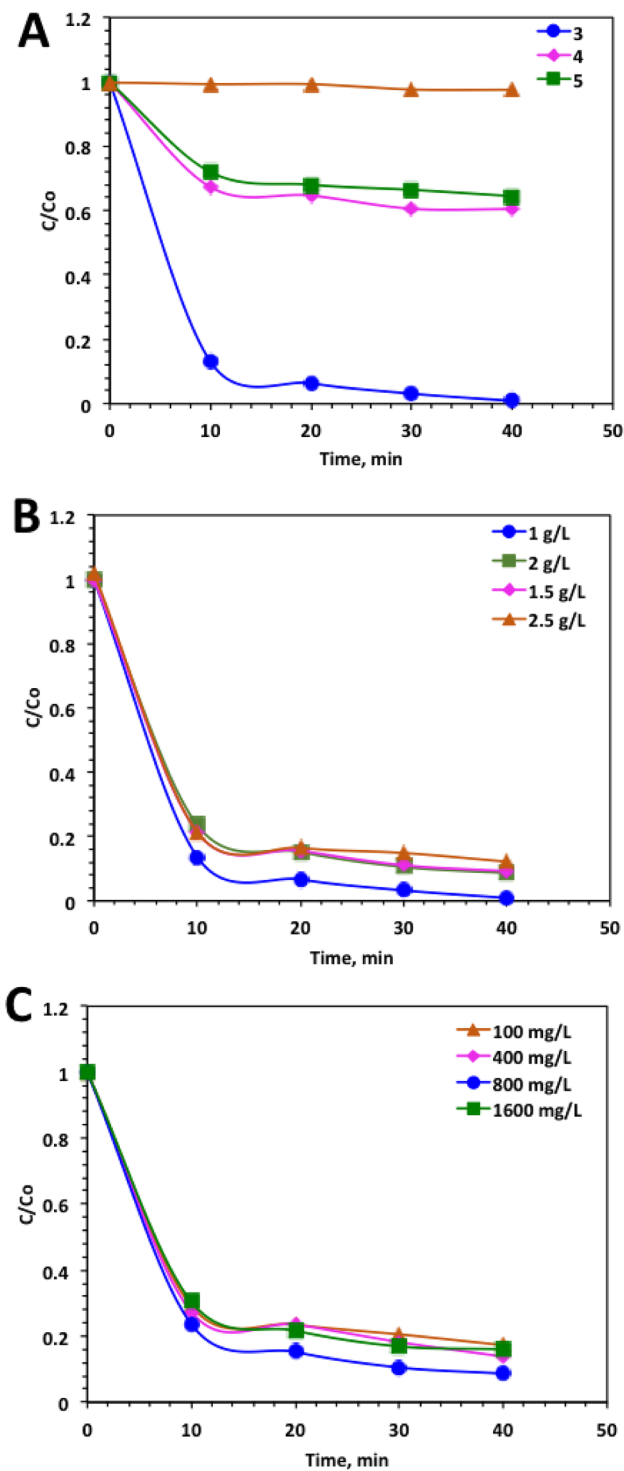
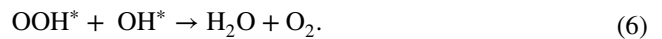
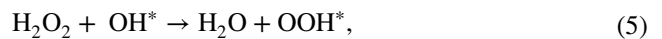


**Fig. 12** Effect of operating parameters on alum sludge photocatalysis system **A** pH (Dye concentration=100 mg/L; H<sub>2</sub>O<sub>2</sub>=800 mg/L); **B** AS400 (Dye concentration=100 mg/L; AS400=0.1 g/L; pH 3.0); **C** H<sub>2</sub>O<sub>2</sub> concentration (Dye concentration=100 mg/L; AS400=0.1 g/L; H<sub>2</sub>O<sub>2</sub>=800 mg/L)

of the catalyst being subjected to UV irradiation and thus, the photocatalytic activity efficiency is declined (Tony and Mansour 2020).

The quantity of H<sub>2</sub>O<sub>2</sub> plays a vital role in the initiation of the photooxidation process, and its effect on the Fenton’s reaction system as well. Figure 12C investigate different values of H<sub>2</sub>O<sub>2</sub> concentration that is ranged from 100 to 1600 mg/L by kept the concentration of AS400 at 2 g/L at pH 3.0. The plot shows that exceeding the concentration of H<sub>2</sub>O<sub>2</sub> results in an increasing in the overall dye removal. However, this observation is reversed at concentration higher or lower than the optimum value (800 mg/L). This may be due to at low H<sub>2</sub>O<sub>2</sub> concentration; there was a deficit in H<sub>2</sub>O<sub>2</sub> to generate sufficient OH free radicals (Tony et al. 2018). However, the exceeds amounts of H<sub>2</sub>O<sub>2</sub> results in OH radical scavenger instead of a producer as shown in the following equations (Thabet et al. 2021a).



**RSM**

In the current study, Alum sludge/Fenton system was revealed to oxidize Levafix dye from simulated textile effluent wastewater under different operating conditions. Three variables, namely, pH, AS400 and H<sub>2</sub>O<sub>2</sub> doses, with three levels of Box–Behnken response surface design were employed to optimize the process performance on the color removal (y) response. The results of the three-level experiments based on a Box–Behnken design are displayed in Table 2. After the data fitting, the following second-order fitting polynomial equation was then further achieved as a quadratic model using SAS software (Eq. 7) and the predicted and experimental data are highly correlated as seen in Fig. 13A.

$$\begin{aligned} \gamma = & 69.92 - 23.9\delta_1 + 2.96\delta_2 + 2.14\delta_3 - 0.52\delta_1^2 \\ & - 0.72\delta_1\delta_2 + 1.82\delta_1\delta_3 - 4.31\delta_2^2 - 0.82\delta_2\delta_3 - 1.11\delta_3^2. \end{aligned} \tag{7}$$

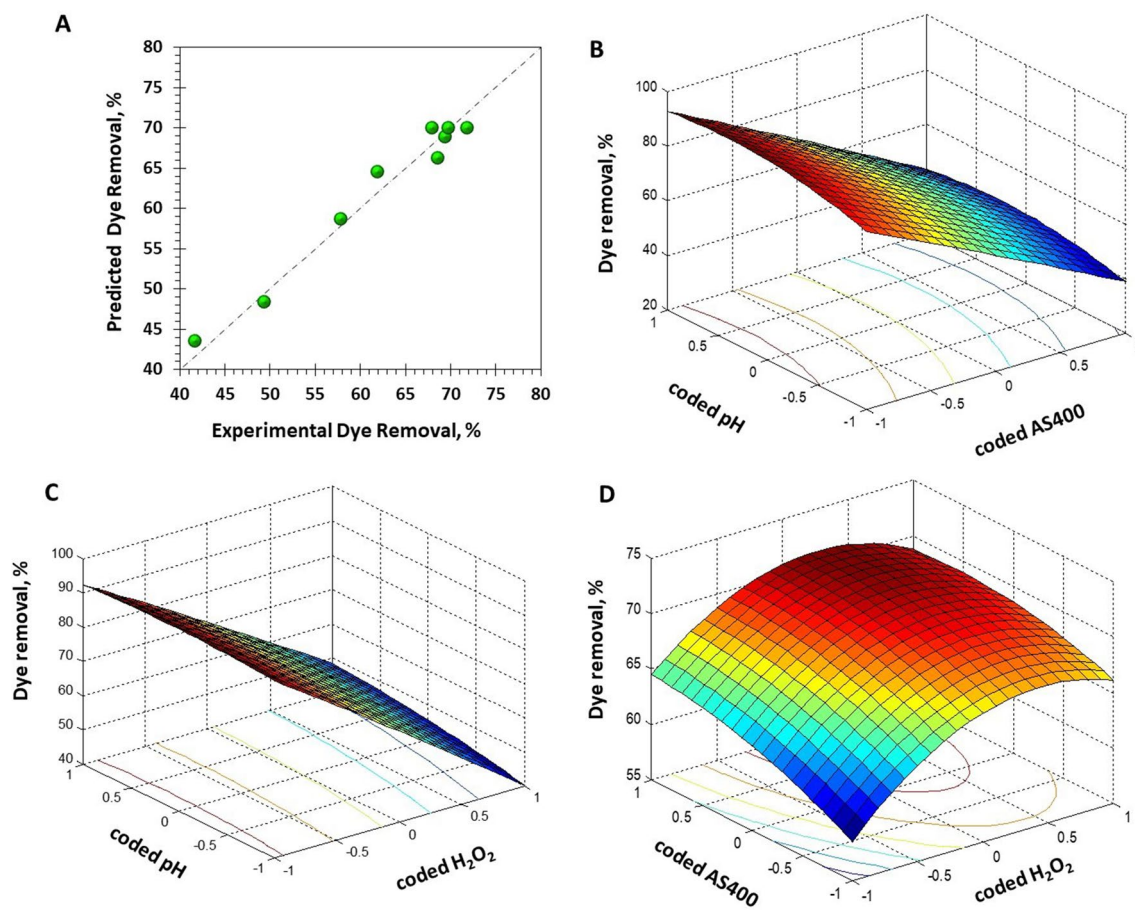


**Fig. 13** Graphical representation of Box–Behnken response surface design for dye oxidation as a function of **A** surface and 2D contour plots of coded pH and AS400 doses; **B** 3D surface and 2D contour

plots of coded pH and H<sub>2</sub>O<sub>2</sub> dose and **D** 3D surface and 2D contour plots AS400 and H<sub>2</sub>O<sub>2</sub> doses

Furthermore, the analysis of variance (ANOVA) test was also examined for the attained response to investigate the predictability of the investigated model. The ANOVA’s data indicate the confident of the model to investigate the dye oxidation. The response surface predictions is in a high correlation coefficient value,  $R^2$  of 99% and 98% for the adj  $R^2$  values. Furthermore, Table 3 tabulated the results of

ANOVA test. The data in the table illustrates that the  $F$  test (Fisher variance ratio) that signifies the parameters explain the sufficient variation of data approaching its mean, and the predicted variable effects are real. The regression model is considered a highly efficient at a too low probability value [probability ( $p$  value) >  $F$  value, 0.0001] (Tony 2020a). As displayed in Table 3, the  $p$ -values of all the coefficients are

**Table 3** ANOVA results for Levafix dye oxidation via alum/Fenton system

Response (y, %)	Source	DF	SS	MS	$F$ value	$P$ value > $F$
Dye removal	Model	9	4766.401	529.6001	76.66178	0.0001
	Linear	3	4677.35531	4677.35531	677.066247	0.093366
	Quadratic	3	16.361223	16.361223	2.368354	1.550506
	Interaction	3	75.939081	75.939081	10.992492	1.034972
	Error	5	34.54134	6.908268		
	Total	14	4800.943			
$R^2 = 99\%$						

$DF$  degrees of freedom,  $SS$  sum of squares,  $MS$  mean of squares ( $MS = SS/DF$ ),  $F$  value of variance,  $P$  value probability of error

less than 0.05; hence, the quadratic regression model shown in Eq. (7) is highly acceptable.

Numerical optimization via Mathematica software (V5.2) was selected to locate the optimum value of the process parameters, i.e., pH, AS400 and  $H_2O_2$  doses to maximize the response (dye removal). The optimum values are located at pH 2.5, 418 mg/L and 1.06 g/L for  $H_2O_2$  and AS400, respectively, with a maximal predicted response of the dye removal of 93.7% after 20 min of reaction time.

Additionally, the model equation Eq. (7) is used to explore the relation between the interacting variables and the response. The response curve and contour plotting are drawn as a function of pH and  $H_2O_2$  doses and displayed in Fig. 13B. As can be understood from the figure, there is one site maximizing the dye removal with maintaining pH at 2.5 and AS400 1.06 g/L addition. Thus, the maximum dye that is oxidized is achieved at the acidic pH conditions. Additionally, the AS400 concentration is relatively influenced by the pH value, and the organics removals raise with the acidic pH and AS400 around 1.0 g/L. Otherwise, the higher pH results in a decrease in the dye oxidation. Consequently, there is an interaction between the AS400 concentration and pH value. The maximum dye removal is corresponding to the optimum values of AS400 and pH. This could be related to the fact that the maximal hydroxyl radical generation is related to the acidic pH which services in initiating the surface of AS400 active sites for reaction (Santana et al. 2019).

Moreover, the excess AS400 declines the oxidation efficiency since it shadows the UV irradiation from penetrating the solution. The interaction effect between the pH and  $H_2O_2$  dose is graphically represented in the 3D surface and 2D contour plots as illustrated in Fig. 13C. There is a clear significant interaction between hydrogen peroxide concentration and pH on the dye oxidation efficiency. Additionally, the excess or may be too low  $H_2O_2$  doses decreases the dye oxidation efficiency through color removal. Also, pH value affects the  $H_2O_2$  decomposition and thus affecting the OH radicals' production, which is the main responsible of the oxidation reaction (Ioannou and Fatta-Kassinos 2013; Tony and Lin 2020b, c, d). The positive influence of the AS400 catalyst dose and the hydrogen peroxide dose on dye oxidation is graphically shown in the 2D and 3D contour and surface plots in the Fig. 13D. As displayed in the Fig. the interaction between the hydrogen peroxide and the AS400 concentrations being in an optimal limit. However, further increase than those concentrations, 1.06 and 418 for AS400 and  $H_2O_2$ , respectively, without regard to the pH operational parameter, the removal efficiency is deduced. Also, as revealed in the surface and contour drawings, decreasing the  $H_2O_2$  and AS400 concentrations lower than those levels results in roughly decrease the dye removal rate. Hence, the dye oxidation and further removal rate is declined at too low or too high AS400 or  $H_2O_2$  reagents doses. This

is confirming the vital role of the optimum reagent values regarding the maximal creation of the (OH) radicals species that are mainly responsible of the significant catalytic oxidation reaction (Dutta et al. 2010).

Finally, to validate the model suitability, three additional replicates of experiments were conducted using maximal predicted values attained via Mathematica software and the experimental response for the maximal dye removal after 20 min of reaction time through Alum sludge/Fenton system measured was 96.5%, respectively, which confirms the model adequacy.

### Thermal Effects on Kinetics and Thermodynamic Profile

Temperature is considered as a key variable that affecting both the reaction rate and the oxidation yield. Therefore, in the second set of experiments, the variation of the temperature in range of 25–60 °C is studied. The data displayed in Fig. 14 exhibited that higher temperature increases the reaction rate between AS400 and  $H_2O_2$ . Therefore, the oxidizing species yield increases, i.e., hydroxyl radicals that have a positive influence on the Levafix molecules oxidation and mineralization. These data indicate that the alum sludge-based Fenton system is dependent on the temperature variation. The quantity of hydroxyl radicals is increased with the temperature elevation. Moreover, AS400 is not only a photocatalyst, but also an adsorbent material (Orlandi et al. 2019). Thus, such adsorption process is highly affected with the temperature increase since the active sites in the AS400 are initiated at high temperature and more cavitation occurs. Those active sites help in expanding the amount of dye removed from wastewater stream. Therefore, this

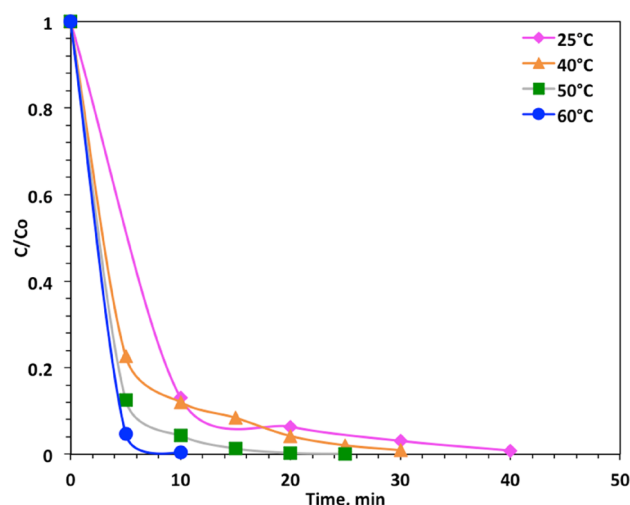


**Fig. 14** Effect of temperature on dual treatment efficiency (Dye concentration = 100 mg/L; AS400 1.0 g/L;  $H_2O_2$  800 mg/L; pH 3.0)

investigation is in accordance with that recommended in the literature (Dutta et al. 2010; Orlandi et al. 2019; Tony 2020a) who suggested the temperature elevation maximizing the oxidation Fenton’s reaction and alum sludge reaction. However, other researchers (Ioannou and Fatta-Kassinou 2013; Pintor et al. 2011) contradict this phenomenon since hydrogen peroxide is very unstable and decomposed by itself at higher temperature. Although such reaction may also occur in the current reaction at high temperature, the hydroxyl radicals production due to the higher temperature reaction between AS400 and H<sub>2</sub>O<sub>2</sub> and the activation of AS400 conducted is more pronounced rather than the hydrogen peroxide decomposition. Hence, the reaction yield is pronounced.

For the object of predicting the performance of the very complex reaction mixture, AS-Fenton system, kinetic modeling was applied to investigate the reaction rate constants. The empirical and theoretical values of zero, first- and second-order kinetic models were compared. The results attained in Table 4. The values of the correlation coefficient, *r*<sup>2</sup>, were used to investigate the various applied models and the best-fit model that is corresponding to the highest correlation coefficient value between the empirical and theoretical data (Lopez-Lopez et al. 2013). Hence, to explore the best fit, the overall correlations were compared and the first-order model that has the quite high *r*<sup>2</sup> values was chosen to describe the results. Although the two models, first- and second-order models, may explain the data, the first-order model has the greatest *r*<sup>2</sup> values (ranged from 0.80 to 0.99). So, the first-order kinetic model can describe the Levafix oxidation via AS-Fenton modified system. Very recently, (Giménez et al. 2021) also found that a first-order reaction model is adequate to describe the Fenton oxidation process. The values of the *k*<sub>s</sub> ranged from 0.04 to 0.57 min<sup>-1</sup>, this

could be illustrated by the temperature change is associated with the difference in the reaction rate and the OH radicals production. Also, the reaction half time (*t*<sub>1/2</sub>) of the Levafix oxidation corresponding to the first-order model increased with the temperature elevation. Therefore, the temperature controlling the reaction of oxidation is verified. Previous data stated in the literature investigating a similar trend (Tony and Lin 2020a).

To give a good understanding of the AS-Fenton oxidation taking place through the ultraviolet oxidation system of Levafix Blue CA dye, thermodynamic parameters were evaluated and the variation of thermodynamic parameters, i.e., Gibbs free energy of activation ( $\Delta G^\circ$ ), activation enthalpy ( $\Delta H^\circ$ ) and activation entropy ( $\Delta S^\circ$ ), with temperature is displayed in Tables 5. The Arrhenius equation,  $k_F = A \exp\left(\frac{-E_A}{RT}\right)$ , was used to calculate the value of energy of activation (*E*<sub>A</sub>), where *A* is the frequency factor, *E*<sub>A</sub> is the activation energy, *R* is the gas constant and *T* is the temperature. The first-order kinetic constant (*k*<sub>F</sub>) is used to calculate the value of energy of activation slope (*E*<sub>A</sub>/*R*) of the Arrhenius plot (plot is not shown) of the reaction rate constant for

**Table 5** Thermodynamic parameters for photocatalytic oxidation of Levafix CA by AS-Fenton

Thermodynamic constant	Temperature (K)			
	298	313	323	333
<i>E</i> <sub>A</sub> (kJ/mol)	61.89			
$\Delta G^\circ$ (kJ/mol)	80.95	81.39	82.64	83.41
$\Delta H^\circ$ (kJ/mol)	59.41	59.28	59.2	59.12
$\Delta S^\circ$ (J/(mol K))	-72.29	-70.62	-72.56	-72.95

**Table 4** Parameters of Zero-, First- and Second-kinetic models for Levafix Blue CA oxidation by alum sludge-based Fenton reaction

Kinetic model	Parameters	Values			
		<i>T</i> (K)			
		298	313	323	333
Zero-order*	<i>K</i> <sub>Z</sub> (min <sup>-1</sup> )	4.67	5.96	6.37	11.56
	<i>t</i> <sub>1/2</sub> (min)	21.39	8.39	7.85	4.33
	<i>r</i> <sup>2</sup>	0.66	0.44	0.33	0.74
Pseudo-first-order**	<i>K</i> <sub>F</sub> (min <sup>-1</sup> )	0.04	0.17	0.29	0.57
	<i>t</i> <sub>1/2</sub> (min)	16.12	4.03	2.32	1.22
	<i>r</i> <sup>2</sup>	0.80	0.98	0.98	0.99
Pseudo-second-order***	<i>K</i> <sub>S</sub> (L mg <sup>-1</sup> min <sup>-1</sup> ) × 10 <sup>-2</sup>	0.04	0.96	11.55	22.50
	<i>t</i> <sub>1/2</sub> (min)	12.5	1.04	0.09	0.04
	<i>r</i> <sup>2</sup>	0.88	0.8	0.59	0.76

\**C*<sub>t</sub> = *C*<sub>0</sub> - *k*<sub>Z</sub>*t*, \*\*(*C*<sub>t</sub> = *C*<sub>0</sub> - *e*<sup>*k*<sub>F</sub>*t*</sup>), \*\*\*( $\frac{1}{C_t} = \left(\frac{1}{C_0}\right) - k_S t$ ), *k*<sub>Z</sub>, *k*<sub>F</sub>, *k*<sub>S</sub> kinetic rate constants of zero-, first- and second-reaction kinetic models, *C*<sub>0</sub> and *C*<sub>t</sub> Levafix concentrations at initial and time *t*, *t* time, *r*<sup>2</sup> correlation coefficient, *t*<sub>1/2</sub> half-life time

AS-Fenton oxidation gives the equivalent activation energy for Levafix Blue CA oxidation of 61.89 kJ/mol. This attained high activation energy more than 40 kJ/mol means a high-energy barrier is needed for oxidizing Levafix dye molecules. This is in accordance with the previously stated by other investigators (Briton et al. 2019; Santana et al. 2019; Tony 2021a) on oxidizing different types of textile dyes from wastewater using Fenton's reaction who recommended that the energy barrier is 79 kJ/mol in mineralizing methylene blue dyed wastewater using nano-haematite catalyst (Mansour et al. 2019). This level of activation energy is well matched with the previously reported data in the literature by Santana (Santana et al. 2019), 107–65 kJ/mol in treating safarin T dye using modified Fenton type. Also, it is similar to the result (55.2 kJ/mol) attained by Briton (Briton et al. 2019) Rhodamine B dye removal using the heterogeneous Fenton type reaction. Commonly, the activation energy of the so-called ordinary thermal reactions is roughly ranged between 60 and 250 kJ/mol (Chen and Zhu 2007) as for advanced oxidation reaction. Thus, the oxidation process could be easily accomplished that recommends the high effectiveness of dye molecules oxidation due the hydroxyl radicals attack regarding the AS-Fenton reaction (Sun et al. 2007). In contrary, (Lin and Leu 1999) recorded low activation energies of 10.62 kJ/mol for oxidizing benzene sulfonate using such reagent. Likewise, (Tony 2021a; Tony and Lin 2020b) observed the low activation energy barrier of 11.104 kJ/mol for treating municipal wastewater.

The Gibbs free energy of activation,  $\Delta G^\circ$ , was calculated to investigate the feasibility of spontaneity of oxidation. The previous integrated relation of the thermodynamic parameter of Gibbs free energy,  $\Delta G^\circ = RT \times \left[ \ln\left(\frac{k_B T}{h}\right) - \ln k \right]$  is applied to calculate the Gibbs free energy of activation where  $k_B$  is Boltzmann's constant,  $h$  is Planck's constant and  $R$  (8.314 J mol<sup>-1</sup> K<sup>-1</sup>) is the gas constant using equilibrium constant  $k_F$  equation. Positive values of the Gibbs free energy of activation  $\Delta G^\circ$  describing the reaction will proceed non-spontaneously. Thus, such non-spontaneous is suggestive endergonic oxidation.

The van't Hoff equation ( $\ln k_F = \frac{-\Delta H}{RT} + \frac{\Delta S}{R}$ ) was used to investigate both values of enthalpy ( $\Delta H^\circ$ ) and entropy ( $\Delta S^\circ$ ). Since  $\Delta H$  and  $\Delta S$  were calculated from the slope and intercept of the van't Hoff plots of  $\ln k_2$  versus  $1/T$  (plot is not included). Negative values of entropy,  $\Delta S^\circ$ , confirm the non-spontaneity of reaction at all temperatures since the values of enthalpy of activation,  $\Delta H^\circ$  are positive. The endothermic process takes place since the values of enthalpy of activation are higher than zero, and the entropy,  $\Delta S^\circ$  of the system decrease with the temperature increase. Thus, elevating the temperature of the system increases the extent of the non-spontaneity of the reaction. Positive values of  $\Delta G^\circ$  verify the process is always non-spontaneous at all temperatures. Also,

negative values of entropy of activation in these cases due to increased randomness at the Levafix dye molecules and the ·OH radicals species produced through the AS-Fenton oxidation reaction and an increase in the degree of freedom of the dye molecules (Parker et al. 2012). Hence, such results are in line with the suggestion that the AS-Fenton reaction mechanisms were energetically stable with a rate of Fenton reaction improved by the temperature increase.

Comparison of different pollutants removal using alum sludge (AS) with other various treatment technologies is displayed in Table 6. It can be concluded that treated alum sludge via Fenton process based on AS as a catalyst attained a full elimination of the pollutant compared to the other literature data. Although previously published electro-Fenton and adsorption treatment methods using alum sludge demonstrated their potential for removing many types of contaminants from wastewater effluents, but they have several drawbacks, such as the requirement for extra chemical reagents and electrical power which increases the expenses of the operation. Also, the main disadvantages for the electro-Fenton process are the use of electrodes that may cause a corrosion to the system. Furthermore, the use of adsorption treatment results in the formation of secondary pollutants because they transmit contaminants from one phase to another without mineralizing them (Thabet et al. 2021b). Furthermore, Kim et al. (2020) and Rashed et al. (2021) who used composites from alum sludge with other materials that show a promising removal for the pollutants but it has a negative impact on the economical part of the process besides the increased sludge and chemicals in the final effluents after treatment. Moreover, these drawbacks are not linked with the present Fenton method suggested for removal of dye. As a result, the recommended approach is considerably superior and less expensive, especially when calcined alum sludge is employed as the source of the Fenton process compared to the other listed techniques in Table 6.

## Conclusion

Fenton reagent could be introduced from alum sludge residue through its simple calcination process and then augmented with the hydrogen peroxide oxidant. The influences of several operational parameters for the AS-based Fenton system, namely, Levafix dye concentration initial concentration, AS dosage, H<sub>2</sub>O<sub>2</sub> concentration, temperature and the solution pH have been evaluated. The best efficiency is obtained for 1.0 g/L of AS samples and 800 mg/L of hydrogen peroxide at the pH 3.0. Whereas, increasing the dye concentration decreasing the overall reaction rate. This study estimates the feasibility of alum sludge waste to be a photocatalyst for treating textile wastewater stream, which may be

**Table 6** Studies on comparison of current study with the recent literature on wastewater treatments using AS via various techniques

AS, source	AS preparation technique	Type of wastewater/Target pollutant	Type of treatment	Test conditions	Removal, %	References
Gezirat El Dabbh Drinking (WTP) in Giza, Egypt	Drying; grinding; calcined (400 °C)	Synthetic wastewater/Levafix Blue CA dye	Photo-Fenton	Co 100 mg/L; pH 3; AS400 1 g/L; H <sub>2</sub> O <sub>2</sub> 800 mg/L; 30 min	99.9	Current study
WTP located in Santa Maria, Brazil	Drying (120 °C); calcined (600 °C); grinding	Synthetic wastewater/ Amaranth dye	Photo-Fenton	Co 50 mg/L; pH 2.8; catalyst 0.75 g/L; H <sub>2</sub> O <sub>2</sub> 5.5 mmol/L; 30 min	97	Grassi et al. (2020)
western Algiers' drinking (WTP) at Algiers, Algeria	Impregnation in iron nitrate; calcined (200–500 °C)	Synthetic wastewater /Reactive blue 19 dye	Photo-Fenton	Co 50 mg/L; pH 3; Fe/DWTR-500 0.5 g/L; H <sub>2</sub> O <sub>2</sub> 10 mM; $I_{UVA} = 3.55 \text{ MW/cm}^2$ ; 120 min	99	Laib et al. (2021)
Saigon Underground Water Company Limited, Vietnam	Dried (103–105 °C)	Real wastewater /dyestuff	Electro-Fenton	pH 4; AS = 2 g; $J = 14 \text{ mA/cm}^2$ ; 90 min	98	Nguyen et al. (2021)
water supply company in Xinjiang, China	Washing; drying; calcined (700 °C)	Synthetic wastewater /Methylene blue dye	Electro-Fenton	Co 20 mg/L; pH 3; AS700 200 g/L; Na <sub>2</sub> SO <sub>4</sub> 0.14 mol/L; $V = 8 \text{ V}$ ; 40 min	91	Yang et al. (2021)
Fatera drinking (WTP) at Kom Ombo, Aswan, Egypt	ASN/TiO <sub>2</sub> composite by sol-gel method	Synthetic wastewater /Rhodamine B dye	Photo-catalysis	Co 50 mg/L; pH 7; ASN/TiO <sub>2</sub> 0.125 g/50 mL; 4 h	97	Rashed et al. (2021)
Drinking (WTP) in Gosan, Wanjju, Korea	Co-pyrolyzed alum sludge/g-C <sub>3</sub> N <sub>4</sub> (550 °C) Composite melamine	Synthetic wastewater/ trivalent arsenic AS(III)	Oxidation /adsorption	Co 1000 mg/L; pH 7; 5 g adsorbent /L; 48 h	37	Kim et al. (2020)
Shebin El-Kom (WTP), Menoufia, Egypt	Dried, calcined (400 °C)	Synthetic wastewater /phenol	Adsorption	Co 100–1000 mg /L;pH 4.5; AS 2 g; 1 h	80%	Tony (2019a)
Drinking (WTP) in Chuncheon city, Korea	Pyrolyzed (700 °C); air-dried (500 °C); oven-dried (105 °C)	Synthetic wastewater/phosphate	Adsorption	Co 12.5 mg/L; pH 7; AS 0.1 g; 48 h	90	Van Truong and Kim (2021)
Shebin El-Kom (WTP), Menoufia, Egypt	Dried; calcined (400 °C)	Synthetic wastewater /procion blue dye	Adsorption	Co 11.8 mg/L; pH 7; AS 2 g; 1 h	91%	Tony (2020b)



recycled in the factory; although, further work is needed to investigate this facility in depth which is not handled through the current study.

**Funding** Open access funding provided by The Science, Technology & Innovation Funding Authority (STDF) in cooperation with The Egyptian Knowledge Bank (EKB). The author(s) received no specific funding for this work.

**Availability of Data and Materials** All data generated or analyzed during this study are included in this published article.

## Declarations

**Conflict of interest** The authors confirm that there is no conflict of interest to declare.

**Consent for publication** The authors confirm the consent for publication.

**Statement of human and animal rights** This article does not contain any studies with human or animal subjects.

**Open Access** This article is licensed under a Creative Commons Attribution 4.0 International License, which permits use, sharing, adaptation, distribution and reproduction in any medium or format, as long as you give appropriate credit to the original author(s) and the source, provide a link to the Creative Commons licence, and indicate if changes were made. The images or other third party material in this article are included in the article's Creative Commons licence, unless indicated otherwise in a credit line to the material. If material is not included in the article's Creative Commons licence and your intended use is not permitted by statutory regulation or exceeds the permitted use, you will need to obtain permission directly from the copyright holder. To view a copy of this licence, visit <http://creativecommons.org/licenses/by/4.0/>.

## References

- Ashour EA, Tony MA (2017) Equilibrium and kinetic studies on biosorption of iron (II) and iron (III) Ions onto eggshell powder from aqueous solution. *Appl Eng* 1:65–73
- Ashour EA, Tony MA (2020) Eco-friendly removal of hexavalent chromium from aqueous solution using natural clay mineral: activation and modification effects. *SN Appl Sci* 2:1–13
- Baltakys K, Jauberthie R, Siauciunas R, Kaminskas R (2007) Influence of modification of SiO<sub>2</sub> on the formation of calcium silicate hydrate. *Mater Sci-Pol* 25:663–670
- Bansal P, Verma A (2017) Synergistic effect of dual process (photocatalysis and photo-Fenton) for the degradation of Cephalexin using TiO<sub>2</sub> immobilized novel clay beads with waste fly ash/foundry sand. *J Photochem Photobiol A* 342:131–142
- Barrer RM (1982) Hydrothermal chemistry of zeolites. *Acad Press* 1:130–140
- Breesem KM, Faris FG, Abidin RZ, Yusof N, Abidin MRZ, Dom NM, Jassam SH, Abdel-Magid IM (2015) Influence of calcination temperatures on microstructures of alum sludge and its pozzolanic properties. *Aust J Basic Appl Sci* 9:181–188
- Briton BGH, Duclaux L, Richardson Y, Yao KB, Reinert L, Soneda Y (2019) Effectiveness of the dispersion of iron nanoparticles within micropores and mesopores of activated carbon for Rhodamine B removal in wastewater by the heterogeneous Fenton process. *Appl Water Sci* 9:1–14
- Brock SL (2004) Nanostructures and nanomaterials: synthesis, properties and applications by Guozhang Cao (University of Washington). Imperial College Press (distributed by World Scientific), London
- Chen J, Zhu L (2007) Heterogeneous UV-Fenton catalytic degradation of dyestuff in water with hydroxyl-Fe pillared bentonite. *Catal Today* 126:463–470
- Chu W (2001) Dye removal from textile dye wastewater using recycled alum sludge. *Water Res* 35:3147–3152
- Dassanayake KB, Jayasinghe GY, Surapaneni A, Hetherington C (2015) A review on alum sludge reuse with special reference to agricultural applications and future challenges. *Waste Manage* 38:321–335
- Dutta B, Jana S, Bhattacharjee A, Gütlich P, Iijima S-I, Koner S (2010)  $\gamma$ -Fe<sub>2</sub>O<sub>3</sub> nanoparticle in NaY-zeolite matrix: preparation, characterization, and heterogeneous catalytic epoxidation of olefins. *Inorg Chim Acta* 363:696–704
- El-Desoky HS, Ghoneim MM, El-Sheikh R, Zidan NM (2010) Oxidation of Levafix CA reactive azo-dyes in industrial wastewater of textile dyeing by electro-generated Fenton's reagent. *J Hazard Mater* 175:858–865
- Espejel-Ayala F, Schouwenaars R, Durán-Moreno A, Ramírez-Zamora RM (2014) Use of drinking water sludge in the production process of zeolites. *Res Chem Intermed* 40:2919–2928
- Exley C (2004) The pro-oxidant activity of aluminum. *Free Radic Biol Med* 36:380–387
- Fungaro DA, Silva MVd (2014) Utilization of water treatment plant sludge and coal fly ash in brick manufacturing. *Am J Environ Prot* 2:83–88
- Geng Y, Zhang J, Zhou J, Lei J (2018) Study on adsorption of methylene blue by a novel composite material of TiO<sub>2</sub> and alum sludge. *RSC Adv* 8:32799–32807
- Ghorpade A, Ahammed MM (2018) Water treatment sludge for removal of heavy metals from electroplating wastewater. *Environ Eng Res* 23:92–98
- Giménez BN, Schenone AV, Alfano OM, Conte LO (2021) Reaction kinetics formulation with explicit radiation absorption effects of the photo-Fenton degradation of paracetamol under natural pH conditions. *Environ Sci Pollut Res* 28:23946–23957
- Grassi P, Drumm FC, Georjin J, Franco DSP, Foletto EL, Dotto GL, Jahn SL (2020) Water treatment plant sludge as iron source to catalyze a heterogeneous photo-Fenton reaction. *Environ Technol Innov* 17:100544
- Ioannou LA, Fatta-Kassinos D (2013) Solar photo-Fenton oxidation against the bioresistant fractions of winery wastewater. *J Environ Chem Eng* 1:703–712
- Kasina M, Wendorff-Belon M, Kowalski PR, Michalik M (2019) Characterization of incineration residues from wastewater treatment plant in Polish city: a future waste based source of valuable elements? *J Mater Cycles Waste Manage* 21:885–896
- Kim J-G, Kim H-B, Yoon G-S, Kim S-H, Min S-J, Tsang DCW, Baek K (2020) Simultaneous oxidation and adsorption of arsenic by one-step fabrication of alum sludge and graphitic carbon nitride (g-C<sub>3</sub>N<sub>4</sub>). *J Hazard Mater* 383:121138
- Laib S, Rezzaz-Yazid H, Yatmaz HC, Sadaoui Z (2021) Low cost effective heterogeneous photo-Fenton catalyst from drinking water treatment residuals for reactive blue 19 degradation: preparation and characterization. *Water Environ Res* 93:1097–1106
- Lee C-I, Yang W-F, Chiou C-S (2006) Utilization of water clarifier sludge for copper removal in a liquid fluidized-bed reactor. *J Hazard Mater* 129:58–63
- Lin SH, Leu HG (1999) Operating characteristics and kinetic studies of surfactant wastewater treatment by Fenton oxidation. *Water Res* 33:1735–1741

- Liu C, Yang YZ, Wan N (2013) Characteristic and mechanisms of chromium (VI) adsorption on alum sludge. *Chin J Environ Eng* 7:97–102
- Liu R, Zhao Y, Sibille C, Ren B (2016) Evaluation of natural organic matter release from alum sludge reuse in wastewater treatment and its role in P adsorption. *Chem Eng J* 302:120–127
- Lopez-Lopez C, Martín-Pascual J, Martínez-Toledo MV, González-López J, Hontoria E, Poyatos JM (2013) Effect of the operative variables on the treatment of wastewater polluted with Phthalo Blue by H<sub>2</sub>O<sub>2</sub>/UV process. *Water Air Soil Pollut* 224:1725
- Lv Q, Li G, Lu H, Cai W, Huang H, Cheng C (2015) Preparation of magnetic zeolite  $\gamma$ -Fe<sub>2</sub>O<sub>3</sub>/TS-1 with core/shell structure and application in photocatalytic degradation. *Micropor Mesopor Mater* 203:202–207
- Mansour SA, Tony MA, Tayeb AM (2019) Photocatalytic performance and photodegradation kinetics of Fenton-like process based on haematite nanocrystals for basic dye removal. *SN Appl Sci* 1:1–8
- Montgomery DC (2017) Design and analysis of experiments. Wiley, Oxford
- Nassar MY, Abdelrahman EA (2017) Hydrothermal tuning of the morphology and crystallite size of zeolite nanostructures for simultaneous adsorption and photocatalytic degradation of methylene blue dye. *J Mol Liq* 242:364–374
- Nassar MY, Ahmed IS, Samir I (2014) A novel synthetic route for magnesium aluminate (MgAl<sub>2</sub>O<sub>4</sub>) nanoparticles using sol–gel auto combustion method and their photocatalytic properties. *Spectrochim Acta Part A Mol Biomol Spectrosc* 131:329–334
- Nguyen DDD, Quang HHP, Nguyen XH, Nguyen TP (2021) The treatment of real dyeing wastewater by the electro-Fenton process using drinking water treatment sludge as a catalyst. *RSC Adv* 11:27443–27452
- Orlandi M, Filosa N, Bettonte M, Fendrich M, Girardini M, Battistini T, Miotello A (2019) Treatment of surfactant-rich industrial wastewaters with concentrated sunlight: toward solar wastewater remediation. *Int J Environ Sci Technol* 16:2109–2114
- Papoulis D (2019) Halloysite based nanocomposites and photocatalysis: a review. *Appl Clay Sci* 168:164–174
- Parker HL, Hunt AJ, Budarin VL, Shuttleworth PS, Miller KL, Clark JH (2012) The importance of being porous: polysaccharide-derived mesoporous materials for use in dye adsorption. *RSC Adv* 2:8992–8997
- Pintor AMA, Vilar VJP, Boaventura RAR (2011) Decontamination of cork wastewaters by solar-photo-Fenton process using cork bleaching wastewater as H<sub>2</sub>O<sub>2</sub> source. *Sol Energy* 85:579–587
- Rashed MN, El Taher MAED, Fadlalla SMM (2021) Photocatalytic degradation of Rhodamine-B dye using composite prepared from drinking water treatment sludge and nano TiO<sub>2</sub>. *Environ Qual Manage*. <https://doi.org/10.1002/tqem.21772>
- Ren N, Subotić B, Bronić J, Tang Y, Dutour Sikirić M, Mišić T, Svetličić V, Bosnar S, Antonić Jelić T (2012) Unusual pathway of crystallization of zeolite ZSM-5 in a heterogeneous system: phenomenology and starting considerations. *Chem Mater* 24:1726–1737
- Roderick M (1997) Color physics for industry. Roderick McDonald, Bradford
- Rozhkovskaya A, Rajapakse J, Millar GJ (2021a) Optimisation of zeolite LTA synthesis from alum sludge and the influence of the sludge source. *J Environ Sci* 99:130–142
- Rozhkovskaya A, Rajapakse J, Millar GJ (2021b) Synthesis of high-quality zeolite LTA from alum sludge generated in drinking water treatment plants. *J Environ Chem Eng* 9:104751
- Ruipérez F, Mujika JI, Ugalde JM, Exley C, Lopez X (2012) Pro-oxidant activity of aluminum: promoting the Fenton reaction by reducing Fe (III) to Fe (II). *J Inorg Biochem* 117:118–123
- Santana CS, Ramos MDN, Velloso CCV, Aguiar A (2019) Kinetic evaluation of dye decolorization by Fenton processes in the presence of 3-hydroxyanthranilic acid. *Int J Environ Res Public Health* 16:1–9
- Shamaki M, Adu-Amankwah S, Black L (2021) Reuse of UK alum water treatment sludge in cement-based materials. *Constr Build Mater* 275:122047
- Strlic M, Kolar J, Selih V-S, Kocar D, Pihlar B (2003) A comparative study of several transition metals in Fenton-like reaction systems at circum-neutral pH. *Acta Chim Slov* 50:619–632
- Sun J-H, Sun S-P, Fan M-H, Guo H-Q, Qiao L-P, Sun R-X (2007) A kinetic study on the degradation of p-nitroaniline by Fenton oxidation process. *J Hazard Mater* 148:172–177
- Tantawy MA (2015) Characterization and pozzolanic properties of calcined alum sludge. *Mater Res Bull* 61:415–421
- Thabet RH, Tony MA, El Sherbiny SA, Ali IA, Fouad MK (2020) Catalytic oxidation over nanostructured heterogeneous process as an effective tool for environmental remediation. *IOP Conf Ser Mater Sci Eng* 975:012004
- Thabet RH, Fouad MK, Ali IA, El Sherbiny SA, Tony MA (2021a) Magnetite-based nanoparticles as an efficient hybrid heterogeneous adsorption/oxidation process for reactive textile dye removal from wastewater matrix. *Int J Environ Anal Chem*:1–23. <https://doi.org/10.1080/03067319.2021.1896716>
- Thabet RH, Fouad MK, El Sherbiny SA, Tony MA (2021b) Synthesis, characterization and potential application of magnetized nanoparticles for photocatalysis of Levafix CA Reactive Azo-Dye in aqueous effluent. *Water Environ J*. <https://doi.org/10.1111/wej.12756>
- Tony M (2019a) Win-win wastewater treatment to sustain world: Porous adsorbents from waste waterworks sludge for phenol remediation. In: Anaerobic digestion conference AD16, the international water association, IWA
- Tony MA (2019b) An industrial ecology approach: green cellulose-based bio-adsorbent from sugar industry residue for treating textile industry wastewater effluent. *Int J Environ Anal Chem* 101:167–183
- Tony MA (2020a) Central composite design optimization of Bismarck Dye oxidation from textile effluent with Fenton's reagent. *Appl Water Sci* 10:1–9
- Tony MA (2020b) Zeolite-based adsorbent from alum sludge residue for textile wastewater treatment. *Int J Environ Sci Technol* 17:2485–2498
- Tony MA (2021a) Low-cost adsorbents for environmental pollution control: a concise systematic review from the perspective of principles, mechanism and their applications. *J Dispers Sci Technol*. <https://doi.org/10.1080/01932691.2021.1878037>
- Tony MA (2021b) Paradigms of homo/heterogeneous Fenton systems incorporating 'Solar Energy' based on 'Emerging Pollutants' removal—challenges, advancements and visualized bibliometric analysis. *Int J Environ Anal Chem*. <https://doi.org/10.1080/03067319.2021.1977287>
- Tony MA (2021c) Solar concentration for green environmental remediation opportunity—international review: advances, constraints and their practice in wastewater treatment. *Int J Environ Anal Chem*:1–33
- Tony MA (2021d) An industrial ecology approach: green cellulose-based bio-adsorbent from sugar industry residue for treating textile industry wastewater effluent. *Int J Environ Anal Chem* 101:167–183
- Tony MA, Lin LS (2020a) Attenuation of organics contamination in polymers processing effluent using iron-based sludge: process optimization and oxidation mechanism. *Environ Technol*. <https://doi.org/10.1080/09593330.2020.1803417>
- Tony MA, Lin LS (2020b) Iron recovery from acid mine drainage sludge as Fenton source for municipal wastewater treatment. *Int J Environ Anal Chem*. <https://doi.org/10.1080/03067319.2020.1734196>

- Tony MA, Lin L-S (2020c) Performance of acid mine drainage sludge as an innovative catalytic oxidation source for treating vehicle-washing wastewater. *J Dispers Sci Technol* 43:1–11
- Tony MA, Lin L-S (2021) Iron coated-sand from acid mine drainage waste for being a catalytic oxidant towards municipal wastewater remediation. *Int J Environ Res* 15:1–11
- Tony MA, Mansour SA (2019) Removal of the commercial reactive dye Procion Blue MX-7RX from real textile wastewater using the synthesized  $\text{Fe}_2\text{O}_3$  nanoparticles at different particle sizes as a source of Fenton's reagent. *Nanoscale Adv* 1:1362–1371
- Tony MA, Mansour SA (2020) Microwave-assisted catalytic oxidation of methomyl pesticide by Cu/Cu<sub>2</sub>O/CuO hybrid nanoparticles as a Fenton-like source. *Int J Environ Sci Technol* 17:161–174
- Tony MA, Zhao YQ, Tayeb AM (2009) Exploitation of Fenton and Fenton-like reagents as alternative conditioners for alum sludge conditioning. *J Environ Sci* 21:101–105
- Tony MA, Zhao YQ, El-Sherbiny MF (2011) fenTon and fenton-like aops for alum sludge conditioning: effectiveness comparison with different  $\text{Fe}^{2+}$  and  $\text{Fe}^{3+}$  salts. *Chem Eng Commun* 198:442–452
- Tony MA, Purcell PJ, Zhao Y, Tayeb AM, El-Sherbiny MF (2015) Kinetic modelling of diesel oil wastewater degradation using photo-fenton process. *Environ Eng Manag J* 14(1)
- Tony MA, Mansour SA, Tayeb AM, Purcell PJ (2018) Use of a fenton-like process based on nano-haematite to treat synthetic wastewater contaminated by phenol: process investigation and statistical optimization. *Arab J Sci Eng* 43:2227–2235
- Tony MA, Parker HL, Clark JH (2019) Evaluating Algibon adsorbent and adsorption kinetics for launderette water treatment: towards sustainable water management. *Water Environ J* 33:401–408
- Van Truong T, Kim D-J (2021) Phosphate removal using thermally regenerated Al adsorbent from drinking water treatment sludge. *Environ Res* 196:110877
- Viljoen EL, Kganyago SV, Ofomaja AE (2021) Size control of cobalt oxide nanoparticles and its effect on the fenton catalytic activity. *Pol J Environ Stud* 30:393–400
- Wang L, Wang W, Liu M, Ge H, Zha W, Wei Y, Fei E, Zhang Z, Long J, Sa R (2019) Understanding structure-function relationships in HZSM-5 zeolite catalysts for photocatalytic oxidation of isopropyl alcohol. *J Catal* 377:322–331
- Wongwichien J, Asavapisit S, Sombatsompop K (2014) Synthesis and use of zeolite Na-A from waste sludge of water treatment plant for ammonium removal. *Studies* 3:7
- Yang Y, Ma C, He X, Li J, Li M, Wang J (2021) Calcined aluminum sludge as a heterogeneous fenton-like catalyst for methylene blue degradation by three-dimensional electrochemical system. *Electrocatalysis* 12:1–17
- Yu Y, Wen W, Qian X-Y, Liu J-B, Wu J-M (2017) UV and visible light photocatalytic activity of Au/TiO<sub>2</sub> nanoforests with Anatase/Rutile phase junctions and controlled Au locations. *Sci Rep* 7:1–13
- Zhao YQ, Keogh C, Tony MA (2009) On the necessity of sludge conditioning with non-organic polymer: AOP approach. *J Residuals Sci Technol* 6:151–155
- Zhao W, Xie H, Li J, Zhang L, Zhao Y (2021) Application of alum sludge in wastewater treatment processes: "science" of reuse and reclamation pathways. *Processes* 9:612